Applied Chemical Engineering (2021) Volume 4 Issue 2
doi:10.24294/ace.v4i2.1344

ORIGINAL RESEARCH ARTICLE

Photocatalytic simultaneous removal of nitrite and ammonia via zinc ferrite/N-doped graphene catalyst

Jia Ye[1,2], Shouqing Liu[1,2*]

[1] *School of Chemistry, Biology and Materials Engineering, Suzhou University of Science and Technology, Suzhou 215009, Jiangsu Province, China*

[2] *Jiangsu Key Laboratory of Environmental Functional Materials, Jiangsu Province, Suzhou 215009, Jiangsu Province, China. E-mail: shouqing_liu@163.com*

ABSTRACT

Zinc ferrite/N-doped graphene catalysts were synthesized by hydrothermal reaction. The synthesized materials were characterized by XRD, TEM, Raman and UV-VIS-DRS. We explored the photocatalytic simultaneous removal of nitrite and ammonia via zinc ferrite/N-doped graphene as the photocatalyst. The effects of pH, amount of catalyst, N-doped graphene content, and initial concentration of ammonia on photocatalytic removal of nitrite and ammonia were examined. The results show that the removal ratio of nitrite–N and ammonia–N is 90.95% and 62.84% respectively, when the dosage of $ZnFe_2O_4$/NG (NG 5.0 wt%) is 1.5 $g \cdot L^{-1}$ and the initial concentrations of nitrite–N 50 $mg \cdot L^{-1}$, ammonia–N 100 $mg \cdot L^{-1}$ with pH 9.5 under anaerobic conditions upon white light irradiation for 3 h. After the solution is aerated for 30 mins and irradiated for 10 h under aerobic conditions, the removal ratios of nitrite–N, ammonia–N and total nitrogen are 92.04%, 89.44% and 90.31% respectively. The complete removal of nigrogen is done.

Keywords: $ZnFe_2O_4$/NG; Nitrite; Ammonia Nitrogen; Photocatalysis; Simultaneous Removal

ARTICLE INFO

Received: 21 May 2021
Accepted: 28 June 2021
Available online: 13 July 2021

1. Introduction

Traditional nitrogen removal technology is the use of microbial nitration and denitrification to treat sewage. Nitrification is to convert Ammonia-N (NH_3-N, simplified as AN) to Nitrite and nitrate by nitrobacteria under anaerobic conditions, and denitrification is to convert Nitrite and nitrate to nitrogen and release it under aerobic conditions to achieve nitrogen removal. However, because microorganisms are greatly affected by environmental temperature, mud year, nutritional composition, and other factors, when the wastewater water quality cannot meet the normal microbial growth conditions, such as heavy metal wastewater, high concentration AN wastewater, carbon-free sewage, and wastewater containing antibiotics are not suitable for biological nitrogen removal, and new nitrogen removal technology needs to be developed[1–3]. The author has reported the method of photocatalytic AN removal[4–8], but studies of photocatalytic simultaneous NN removal (NN-N, NO_2^--N, simplified as NN) and AN have rarely been reported[9]. The author used $ZnFe_2O_4$ as the main catalyst to obtain a zinc iron/nitrogen miscellaneous graphene ($ZnFe_2O_4$/NG) hybrid photocatalyst prepared by loading nitrogen miscellaneous graphene (NG). Using this

hybrid photocatalyst, the study of simultaneous photocatalytic removal of NN and AN was carried out, and the process conditions of simultaneous removing NN and AN were optimized.

2. Experimental section

2.1 Chemical reagent

$Fe(NO_3)_3 \cdot 9H_2O$ was purchased from Tianjin Damao Chemical Reagent Factory; $Zn(NO_3)_2 \cdot 6H_2O$ and $KMnO_4$ were purchased from Nanjing Chemical Reagent Factory; NaOH and graphite powder was purchased from Shanghai Reagent General Factory, China; $CO(NH_2)_2$ was purchased from Shanghai Epei Chemical Reagent Co., Ltd.

2.2 Preparation of GO oxide

GO was first synthesized using a modified Hummers method[10], accurately weighing 1.0 g of graphite powder (washed 2–3 times with 5% dilute hydrochloric acid, washed to neutral with deionized water) in a 500 mL beaker, placed in a water bath and stirred continuously in ice water (0 ℃). Add the exact amount of 15.0 mL of thick sulfuric acid to the graphite powder suspension and mix. Potassium permanganate was taken for 3.0 g accurately, and add the above mixture was slowly. Stir for 30 min with the control temperature not exceeding 20 ℃. Take 45 mL deionized water, add the above mixture into it slowly, stir it well, then slowly add hydrogen peroxide solution (10%, 150 mL) into it and stir it for 24 h at room temperature. Calm down, washed to neutral, and the lower mixture was taken and dried in a 60 ℃ vacuum drying tank for 24 h, namely GO.

2.3 Preparation of NG

The 80 mg of GO was accurately weighed and sonicated and dispersed in 50 mL of deionized water. Accurately take 24.0 g of urea and add it to the above solution, mix evenly with water to 80 mL, sonicate it for 60 min, after which transfer it to a high pressure water heat reactor and seal it at 170 ℃ for 12 h. Samples were cooled to room temperature, washed, filtered with deionized water, and dried in a 60 ℃ vacuum drying tank for 24 h, namely NG.

2.4 Synthesis of the $ZnFe_2O_4$/NG

The solution was dissolved in 20.0 mL deionized water with magnetic stirring of 1.7850 g $Zn(NO_3)_2 \cdot 6H_2O$ (6 mmol) and 4.8480 g $Fe(NO_3)_3 \cdot 9H_2O$ (12 mmol). An amount of 72.3 mg NG ($ZnFe_2O_4$ 5.0 wt%) was dissolved in 10 mL of deionized water for 1 h, zinc salt, and the iron salt mixture was added to the NG suspension and stirred magnetically for 1 h. An exact amount of 2.40 g of sodium hydroxide was dissolved in 10 mL of deionized water, slowly added to the above suspension and stirred for 1.5 h. Eventually, the total volume of the solution was about 60 mL. The suspension was transferred to a 100 mL stainless steel high-pressure reactor, and placed in the oven heated up to 180 ℃ for 8 h. The samples naturally cooled to room temperature, then washed, filtered, and dried in a 60 ℃ vacuum drying tank for 24 h namely the $ZnFe_2O_4$/NG hybrid photocatalyst. Similarly, the $ZnFe_2O_4$ can be prepared.

2.5 Catalyst characterization

The X-ray powder diffraction method (XRD, X-ray powder diffraction instrument, Model: D/max 2500 pC type) characterizes the crystal phase structure of the catalyst. The X-ray source is a Cu-Kα, radiation wavelength of 0.154 nm and a tubes voltage and tube current of 40 kV, 40 mA., respectively Transmission electron microscopy (TEM, Model TecnaiG220, FEI, USA) were used to characterize the catalyst morphology and particle size. The diffuse spectra of the samples were determined by UV-visible diffuse spectroscopy (UV-Vis DRS, UV-visible diffuse spectrometer, model: Shim UV 3600 plus type). Raman spectra of the samples (Model Type LabRam HR800, Raman spectrometer) were determined at 633 nm laser excitation.

2.6 Photocatalytic nitride removal assay

First dissolved oxygen was removed by N_2 bubble 30 min to form an anaerobic environment, after the addition of 50 $mg \cdot L^{-1}$ NO_2^--N and 100 $mg \cdot L^{-1}$ NH_3-N, about pH = 9.5 after 1 $mol \cdot L^{-1}$ NaOH of the regulatory reaction solution, and then 0.375 g of catalyst was added. Using a 300 W mercury lamp as a

light source, photocatalytic experiments were carried out in a photocatalytic reactor (BL-GHX-V, Shanghai Bililang Instruments Co., Ltd.), where a reaction temperature of around 25 ℃ was maintained through a quartz cold trap as shown in **Figure 1**. The concentration of the first anaerobic photocatalytic reaction of NN, AN, and NO-N was measured by 3 mL solution for 3 h at 30 min. During the detection process, NN, NO-N, and AN were detected respectively to avoid mutual interference. The analysis of NN was determined by N-(1-Nokia) ethyl diamine photometric method, NN by UV spectrophotometric method, AN using the national standard nano reagent colorization method. To achieve complete removal of NN and AN, the remaining AN solution was aerated for 30 min to form an aerobic environment, and at the second phase of the photocatalytic reaction, while using sodium hydroxide to maintain about pH = 9.5, remove the residual AN, to achieve omplete removal of total nitrogen.

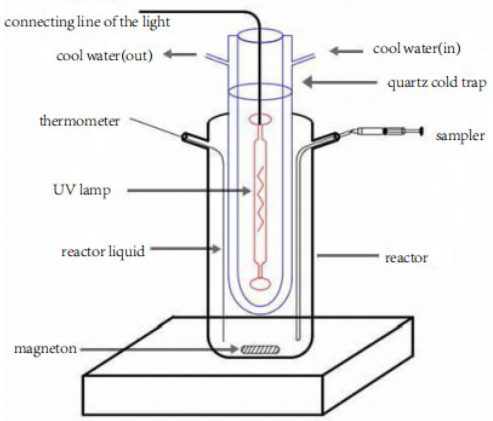

Figure 1. Experimental device for photocatalytic simultaneous removal of NN and AN.

2. Results and discussion

2.1 X-ray powder diffraction characterization

Figure 2 is a diffraction map of XRD for NG, $ZnFe_2O_4$, $ZnFe_2O_4$/NG. Curve a is a diffraction map of NG, with diffraction peaks at 2θ = 29.84, 35.14, 42.77, 53.06, 56.59, 61.98, 70.13, 73.58 and 78.35° corresponding to the $ZnFe_2O_4$ diffraction surface (220), (311), (400), (422), (511), (440), (620), (533) and (444), respectively, consistent with the $ZnFe_2O_4$ standard map (JCPDS22-1012). The comparison curves (b) and (c) show that the diffraction pattern of $ZnFe_2O_4$/NG is basically consistent with that of $ZnFe_2O_4$. At the same time, the diffraction peak of (002) plane of NG is observed at 26.2° in the $ZnFe_2O_4$/NG diffraction pattern, indicating that NG is well dispersed in the catalyst.

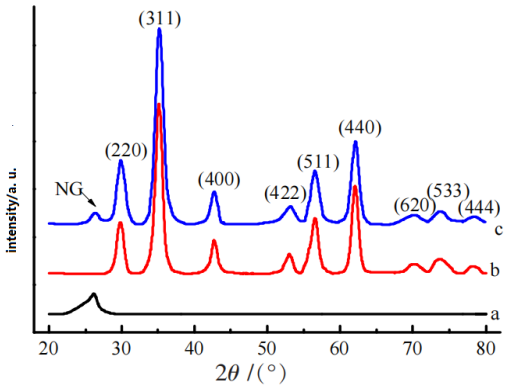

Figure 2. XRD Atlas (a: NG; b: $ZnFe_2O_4$; c: $ZnFe_2O_4$/NG).

According to the half-peak width of the diffraction peak of the crystal surface (311) in curves b and c and the Scherrer formula D = Kλ/(Wcosθ), we can calculate the particle size of the $ZnFe_2O_4$/NG, $ZnFe_2O_4$. D is the average particle size of the grain; K is the grain shape factor, 0.89 as its value; X-ray wavelength, 0.154 nm as its value; W is the half-peak width of the diffraction peak; andθis the diffraction angle. The particle size of $ZnFe_2O_4$/NG, $ZnFe_2O_4$ was 6.9 and 7.2 nm, respectively, consistent with the TEM observations.

3.2 Transmission electron microscope

Figure 3 is TEM diagram at different resolutions of NG, $ZnFe_2O_4$, $ZnFe_2O_4$/NG. NG is a two-dimensional layered structure (**Figure 3a**). **Figure 3b** Zinc iron acid is granular with a uniform size of about 6-9 nm, consistent with the XRD analysis, while the $ZnFe_2O_4$ is better distributed on the NG surface. **Figure 3c** clearly shows the lattice stripes with a lattice stripe spacing of 0.25 nm corresponding to the stripe spacing of the $ZnFe_2O_4$ (JCPDS22-1012) (311) faces.

3.3 Raman spectral characterization

Figure 4 shows the Raman spectrogram of all the NG, $ZnFe_2O_4$ and $ZnFe_2O_4$/NG. **Figure 4a** shows bands D and G of NG. Three characteristic peaks are clearly observed in **Figure 4b**: 339, 474, 665 cm^{-1},

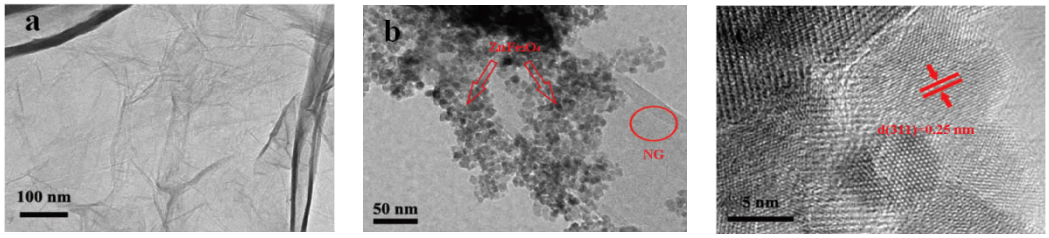

Figure 3. Transmission electron microscope diagram (a: NG; b and c: $ZnFe_2O_4$/NG).

corresponding to the classical vibration mode of the spinel structure, further demonstrating that $ZnFe_2O_4$ is a spinel structure[11,12]. Two characteristic peaks were observed at 1,567 cm^{-1} and 1,334 cm^{-1} representing band G and D of graphene, respectively, 1,567 cm^{-1} (band G) as graphene E_{2g} vibration mode, and 1,334 cm^{-1} (band D) associated with defects and irregularity of graphite structures[12,13]. The good binding of $ZnFe_2O_4$ to the Raman peak of NG as observed in **Figure 4c** further confirms the presence of NG in the $ZnFe_2O_4$ hybridization.

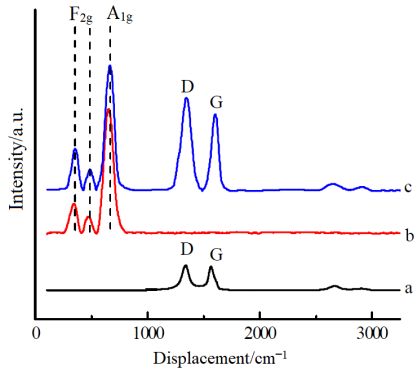

Figure 4. Raman Spectrogram (**a**: NG; **b**: $ZnFe_2O_4$; **c**: $ZnFe_2O_4$/NG).

3.4 UV-visible diffuse spectroscopy characterization

Figure 5 is the DRS spectra for the $ZnFe_2O_4$/NG and $ZnFe_2O_4$ samples. **Figure 5A** shows the UV-visible diffuse spectra. It shows from **Figure 5A** that $ZnFe_2O_4$/NG shows absorption enhancement in the wavelength range greater than 530 nm, meaning that the NG load improves the absorption efficiency of incoming photons, broadens the response range to visible light, effectively suppresses the combination of photosynthetic electrons and photosynthetic holes, and greatly improves the utilization rate of solar irradiation.

By the Tauc formula, we can calculate band widths of $ZnFe_2O_4$/NG and $ZnFe_2O_4$,

$$(\alpha h\nu)^2 = A(h\nu - E_g)$$

in which, A is the proportional constant; the absorption coefficient; the frequency of light; h is the Planck constant; E_g is the semiconductor forbidden band width. **Figure 5B** is the corresponding (h) 2-h plot, available by **Figure 5B**, band widths of $ZnFe_2O_4$/NG and $ZnFe_2O_4$ are 2.0 and 2.1 eV, respectively. After the $ZnFe_2O_4$ catalyst loads nitrogen and miscellaneous graphene, the spectral absorption wavelength occurs at redshift and the width of the forbidden band decreases, therefore, improves the absorption utilization of solar energy.

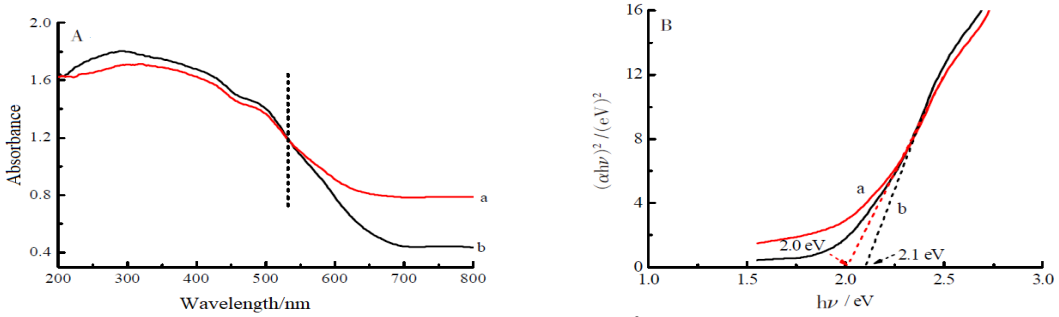

Figure 5. UV-visible diffuse spectroscopy (A), corresponding $(\alpha h\nu)^2$ and h plot (B) (a: $ZnFe_2O_4$/NG; b: $ZnFe_2O_4$).

3.5 Photocatalysis simultaneously removes NN and AN

3.5.1 Simultaneous removal of nitrous nitrogen and AN

Figure 6 is the removal curve for NN in light or

dark reaction or absence of a component, **Figures 6A** and **6B** show the removal curves for NN and AN, respectively. Use 1.5 g·L^{-1} $ZnFe_2O_4$/NG (NG 5.0 wt%) as the catalyst, and the initial solution volume was 250.0 mL, NN and AN was 50 mg·L^{-1}, 100 mg·L^{-1} and pH = 9.5, respectively. The corresponding conditions in the figure are: (a) NN + AN + $ZnFe_2O_4$/NG + illumination; (b) NN + AN + illumination; (c) NN + $ZnFe_2O_4$/NG + illumination; (d) NN + AN + $ZnFe_2O_4$/NG; (e) AN + $ZnFe_2O_4$/NG +illumination. **Figure 6A (a)**, **6B (a)** show that the removal rates of NN and AN was 90.95% and 62.84% in the presence of catalyst, respectively. However, curves 6A (b), 6B (b) show that the removal of nitrogen was only 20.53% and 18.75% even with light in the condition that there is not catalyst. This shows that the catalyst has photocatalytic activity to simultaneously remove NN and AN. When the reaction system lacked AN, only 1.03% nitrogenous nitrogen was adsorbed by the catalyst, as shown in **Figure 6A (c)**. However, when NN was absent in the reaction system, the catalyst adsorbed only 11.96% of the AN, as shown in **Figure 6B (e)**. In light-free conditions, even in the presence of a photocatalyst, only a small amount of NN was adsorbed with AN, as shown in **Figures 6A (d)** and **6B (d)**. By comparison, $ZnFe_2O_4$/NG catalyst can remove NN and AN simultaneously under anaerobic conditions.

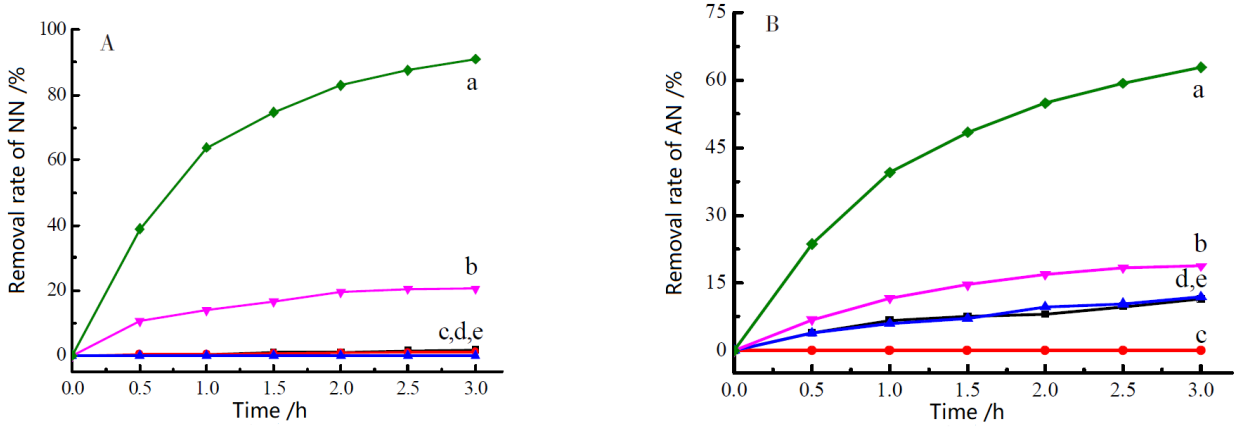

Figure 6. Elimination curves of the NN and AN.

3.5.2 Effect of the pH-values

The pH value of the solution was adjusted at 1.0 mol·L^{-1} NaOH, 0.375 g $ZnFe_2O_4$/NG (NG 5.0 wt%) was added to a mixture of 50 mg·L^{-1} NN and 100 mg·L^{-1} AN, white light for different pH for 3 h, and the removal effect of NN is shown in **Figure 7**. The removal rate of NN and AN increased with increasing solution pH. When pH was 9.50, NN and AN reached the optimal value of 90.95% and 62.84%, respectively.

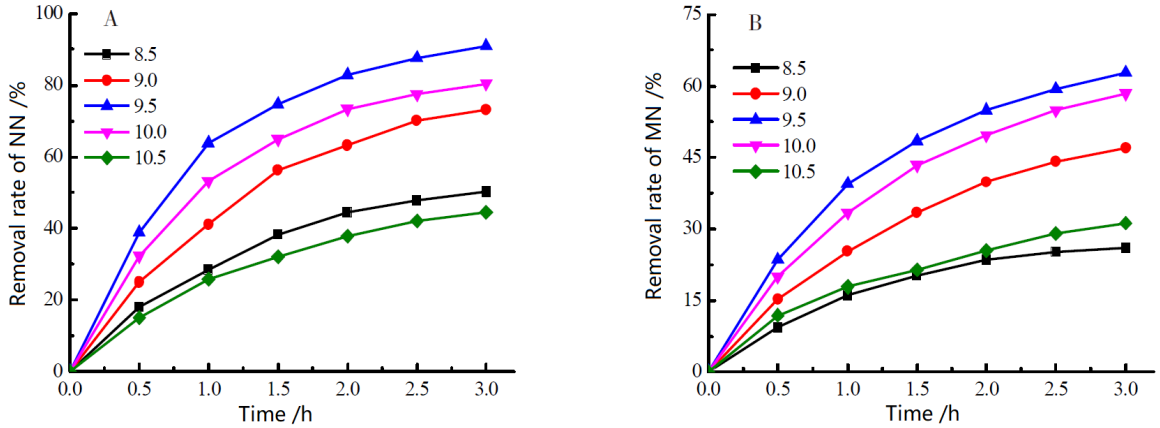

Figure 7. Effect of pH values on the removal efficiency of nitrogenous nitrogen (A) and AN (B) (50.0 mg·L^{-1} NN + 100.0 mg·L^{-1} AN + 0.375 g·L^{-1} $ZnFe_2O_4$/NG, solution volume is 250.0 mL).

3.5.3 Effect of the catalyst dosage

In a mixture of pH = 9.5, NN 50 mg·L^{-1}, of AN 100 mg·L^{-1}, 0.125 of 0.25, 0.25, 0.375, 0.5 g $ZnFe_2O_4$/NG hybrid catalysts were added, white light irradiated for 3 h, and the removal efficiency of NN and AN is shown in **Figure 8**. With the increasing amount of catalyst consumption, the removal rate of NN and AN also increases. When the catalyst dosage was 1.5 g·L^{-1}, the removal rate of NN and AN was optimal, which were 90.95% and 62.84%, respectively. When the catalyst dosage continues to increase, the removal rate decreases instead. Analysis of the reasons, perhaps due to excessive catalyst consumption, reunion phenomenon, resulting in reduced removal rate.

3.5.4 Effect of the NG load

The efficiency of $ZnFe_2O_4$/NG carrying different proportions of NG (0%–9%) as the catalyst, under pH of 9.5, and the simultaneous removal of NN and AN for 3 h is shown in **Figure 9**. The simultaneous removal of nitrogenous nitrogen and AN was 81.19% and 54.70%. Under the same experimental conditions, the NN and AN removal rate increased with the NG ratio. When the NG load was 5%, the removal rate of NN and AN reached the best value of 90.95% and 62.84%, respectively.

3.5.5 Effect of the initial concentration of AN on the denitrification rate of NN

The effect of the initial AN concentration on NN reduction was explored by controlling the pH (9.50), catalyst dosage (1.5 g·L^{-1}), NG load (5%), and catalytic reaction time (3 h), as shown in **Figure 10**. Experimental results show that the rate of NN increases with the initial concentration of AN. When the initial concentration of AN was 100 mg·L^{-1}, the NN removal rate reached 90.95%. Similar to results of AN. When the initial concentration of AN was 100 mg·L^{-1}, the removal rate reached 62.84%.

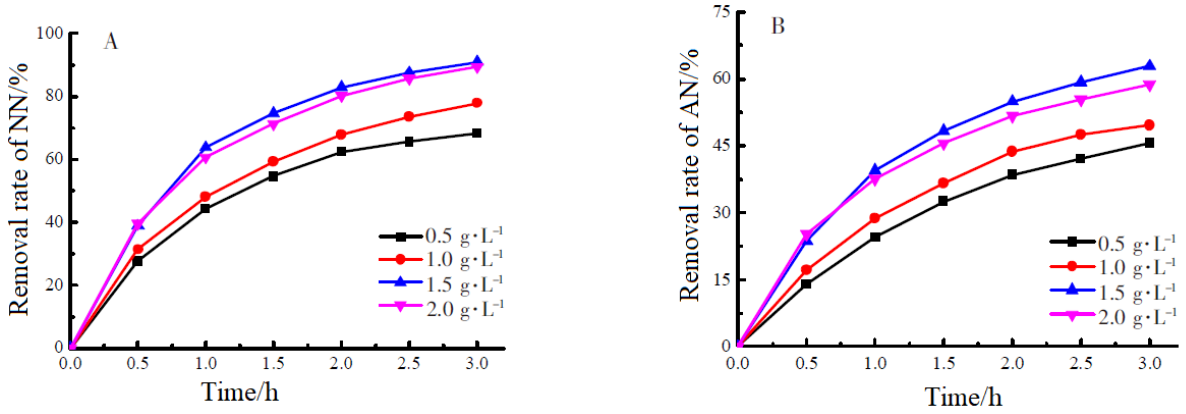

Figure 8. Effect of the catalyst dosage on the removal efficiency of nitrogenous nitrogen (A) and AN (B).

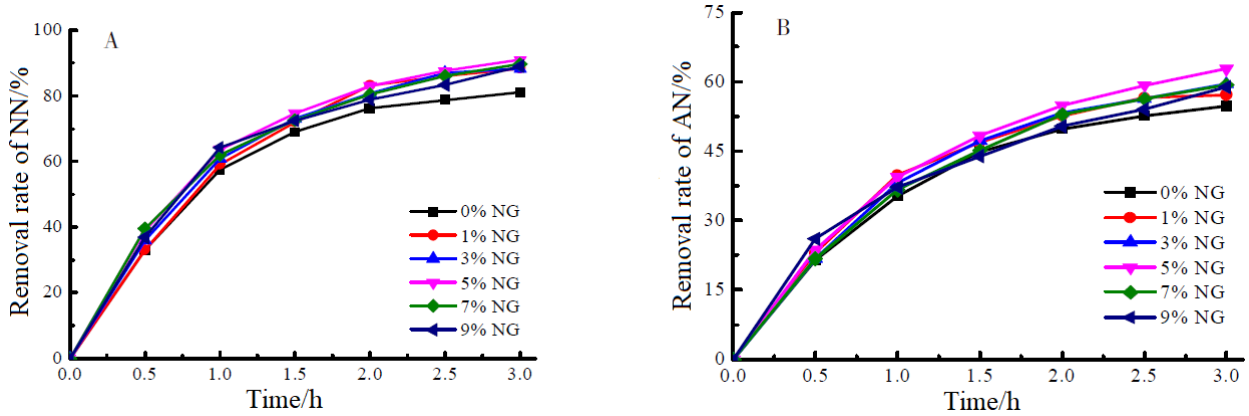

Figure 9. Effects of NG load on the removal efficiency of nitrogenous nitrogen **(A)** and AN **(B)** (50.0 mg·L^{-1} NN + 100.0 mg·L^{-1} AN + 1.5 g·L^{-1} $ZnFe_2O_4$/NG, Solution Volume 250.0 mL, pH = 9.5).

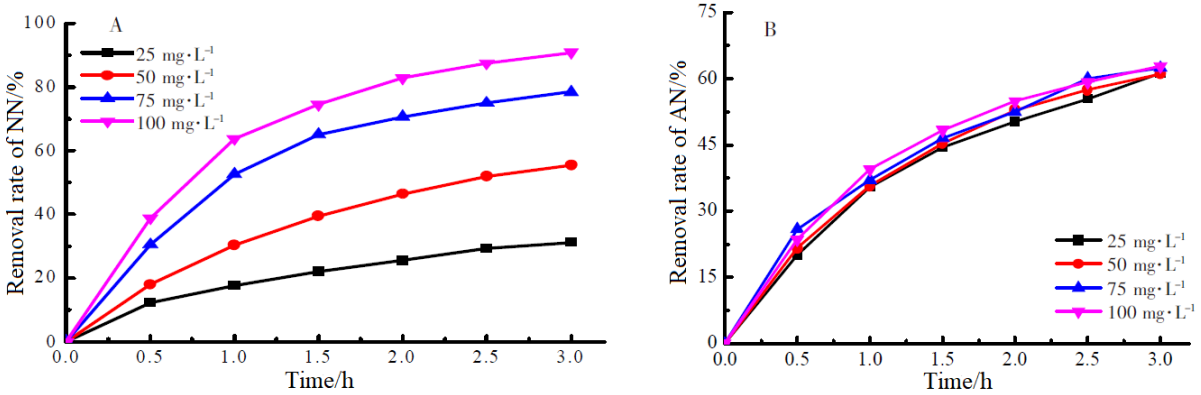

Figure 10. Effect of initial concentration on NN rate (A) and B) (50.0 mg·L^{-1} NN + AN + 1.5 g·L^{-1} $ZnFe_2O_4$/NG, solution 250.0 mL, pH = 9.5).

3.5.6 Catalyst stability and reuse

Figure 11 is the circle experiment of removing NN and AN under white light irradiation. After 7 cycle experiments, the removal rate of nitrogenous nitrogen was 87.28%. This indicates that the $ZnFe_2O_4$/NG hybridization catalyst is well stable and recyclable.

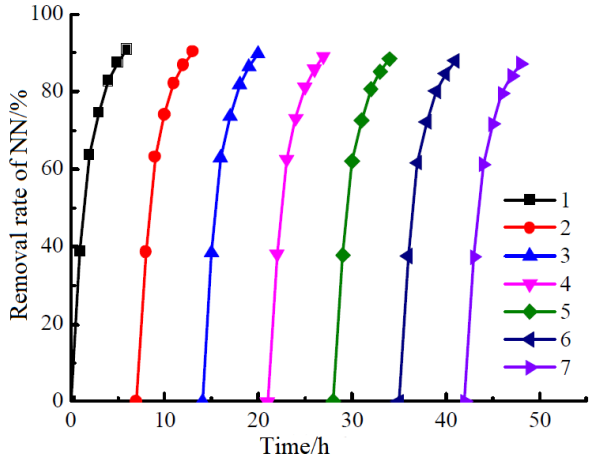

Figure 11. Catalyst recycling test diagram (50.0 mg·L^{-1} NN + 100.0 mg·L^{-1} AN+1.5 g·L^{-1} $ZnFe_2O_4$/NG, Solution volume 250.0 mL, pH = 9.5).

3.5.7 Complete denitrification

Figure 12 is the plot of the removal rate of nitrogenous nitrogen and AN. The experimental design was divided into two phases, the first study of photocatalytic removal of NN and AN under anaer obic conditions, with removal rates of 90.95% and 62.84% respectively. The AN with about 37 mg·L^{-1} remaining in the solution was not removed. The second stage is to aerate the solution for 30 min and continue the above reaction to remove the remaining AN. The results are shown in **Figure 12**, and the removal rates of NN, AN, and total nitrogen reached 92.04%, 89.44%, and 90.31% after the 13th h of light, respectively. No NN generation was detected during the photocatalytic reaction.

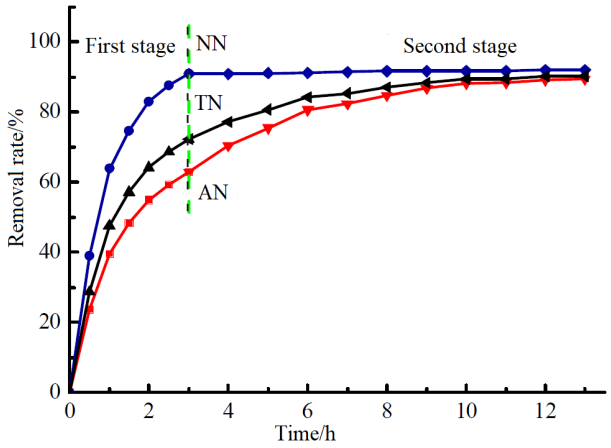

Figure 12. Change curves of both Nitrogen and AN (50.0 mg·L^{-1} NN + 100.0 mg·L^{-1} AN + 1.5 g·L^{-1} $ZnFe_2O_4$/NG, Solution Volume 250.0 mL, pH = 9.5).

3.5.8 Reaction mechanism

Since the width of $ZnFe_2O_4$/NG forbidden band is 2.0 eV and its conduction band potential is E_c = –0.9 V vs NHE[4], and NN reduced potential is $E^0_{NO_2^-/N_2}$ = 1.52 V vs NHE. The photosynthetic electrons can reduce NN ions to nitrogen. The valence band potential of $ZnFe_2O_4$/NG is E_v = 1.1 V vs NHE, and the oxidation potential of AN is $E^0_{N_2/NH_3}$ = 0.057 V vs NHE, so the photosynthetic hole can oxidize AN to nitrogen. The total reactivity formula is: $NO_2^- + NH_3 + H^+ = N_2 + 2H_2O$.

4. Conclusions

$ZnFe_2O_4$/NG hybrid photocatalyst synthesized by the hydro heat method. The experiment of photocatalytic removal of NN and AN carried out. Experexperiment showed that in mixed NN and AN with pH = 9.5, the initial concentration of 1.5 $g \cdot L^{-1}$, NN and $ZnFe_2O_4$/NG (NG 5.0 wt%) was 50 and 100 $mg \cdot L^{-1}$, respectively, for 3 h, and the removal rate of NN was the largest, with 90.95% and 62.84%, respectively. The solution was aerated for 30 min and continuous illumination 10 h, the removal rates of NN, ammonia, and total nitrogen reached 92.04%, 89.44%, and 90.31%, respectively, which indicates the potential application of $ZnFe_2O_4$/NG hybridization catalyst for photocatalytic removal of NN and AN.

Conflict of interest

The authors declare that they have no conflict of interest.

Acknowledgements

Fund project: supported by the National Natural Science Foundation of China (21576175); Jiangsu industry foresight project (be2015190); Graduate innovation project of Suzhou University of science and Technology (skcx16_066).

References

1. Yang J, Xu K. Microbiology in sewage treatment (in Chinese). Science and Technology & Innovation 2017; (12): 71.
2. Zhang L, Xu J, Qiao X. New process for high-concentration AN wastewater treatment (in Chinese). Process 2017; (10): 20–22.
3. Wei N, Zhao S, Sun Y, *et al.* Strategies for dosing carbon source for enhanced nitrogen removal in wastewater treatment plant. China Water & Wastewater 2017; 33(1): 71–75.
4. Liu S, Zhu X, Zhou Y, *et al.* Smart photocatalytic removal of ammonia through molecular recognition of zinc ferrite/reduced graphene oxide hybrid catalyst under visible-light irradiation. Catalysis Science & Technology 2017; 7(15): 3210–3219.
5. Zhang H, Liu S. Catalytic properties of graphene/molybdenum sulfide under near-infrared light irradiation. Journal of Suzhou University of Science and Technology (Natural Science Edition) 2017; 34(4): 37–41, 53.
6. Xue T, Zhang H, Liu S. Synthesis of reduced graphene oxide-cerium oxide hybrid catalyst and the degradation of ammonia under visible light irradiation. Journal of Functional Materials 2017; 48(3): 3218–3222.
7. Zou C, Liu S, Shen Z, *et al.* Efficient removal of ammonia with a novel graphene-supported $BiFeO_3$ as a reusable photocatalyst under visible light. Chinese Journal of Catalysis 2017; 38(1): 20–28.
8. Xiao B, Liu S. Photocatalytic oxidation of ammonia via an activated carbon-nickel ferrite hybrid catalyst under visible light irradiation. Acta Physico-Chimica Sinica 2014; 30(9): 1697–1705.
9. Kominami H, Kitsui K, Ishiyama Y, *et al.* Simultaneous removal of NN and ammonia as zinitrogen in aqueous suspensions of a titanium (IV) oxide photocatalyst under reagent-free and metal-free conditions at room temperature. RSC Advances 2014; 46(7): 51576–51579.
10. Liu S, Xiao B, Feng L, *et al.* Graphene oxide enhances the Fenton-like photocatalytic activity of nickel ferrite for degradation of dyes under visible light irradiation. Carbon 2013; 64(9): 197–206.
11. Wang Z, Schiferl D, Zhao Y, *et al.* High pressure Raman spectroscopy of spinel-type ferrite $ZnFe_2O_4$. Journal of Physics and Chemistry of Solids 2003; 64(12): 2517–2523.
12. Yang C, Li Z, Yu L, *et al.* Mesoporous zinc ferrite microsphere-decorated graphene Oxide as a flame retardant additive: preparation, characterization, and flame retardance evaluation. Industrial & Engineering Chemistry Research 2017; 56(27): 7720–7729.
13. Akhavan O. The effect of heat treatment on formation of graphene thin films from graphene oxide nanosheets. Carbon 2010; 48(2): 509–519.